Universal scaling of nonlinear conductance in the two-channel pseudogap Anderson model: Application for gate-tuned Kondo effect in magnetically doped graphene

Tsung-Han Lee,[1] Kenneth Yi-Jie Zhang,[1] Chung-Hou Chung,[1,2] and Stefan Kirchner[3,4]
[1] *Electrophysics Department, National Chiao-Tung University, HsinChu, Taiwan, 300, Republic of China*
[2] *National Center for Theoretical Sciences, HsinChu, Taiwan, 300, Republic of China*
[3] *Max-Planck-Institut für Physik Komplexer Systeme, 01187 Dresden, Germany*
[4] *Max-Planck-Institut für Chemische Physik fester Stoffe, 01187 Dresden, Germany*
(Received 24 March 2013; revised manuscript received 12 July 2013; published 26 August 2013)

Based on the noncrossing approximation, we calculate both the linear and nonlinear conductance within the two-lead two-channel single-impurity Anderson model where the conduction electron density of states vanishes in a power-law fashion $\propto |\omega - \mu_F|^r$ with $r = 1$ near the Fermi energy, appropriate for a hexagonal system. For given gate voltage, we address the universal crossover from a two-channel Kondo phase, argued to occur in doped graphene, to an unscreened local moment phase. We extract universal scaling functions in conductance governing charge transfer through the two-channel pseudogap Kondo impurity and discuss our results in the context of a recent scanning tunneling spectroscopy experiment on Co-doped graphene.

DOI: 10.1103/PhysRevB.88.085431 PACS number(s): 73.61.Ph, 73.40.−c, 73.50.−h, 73.63.Rt

I. INTRODUCTION

The two-channel Kondo[1] (2CK) problem[2] is a fascinating example of an exotic quantum many-body phenomenon resulting in a metallic ground state with non-Fermi-liquid behavior. It involves a single quantum impurity spin with $s = 1/2$ that couples antiferromagnetically to two identical conduction electron reservoirs. As a result, Kondo processes involving both reservoirs lead to overscreening of the local moment. Theoretically, the two-channel Kondo physics has been studied extensively via Bethe ansatz,[3] conformal field theory,[4] bosonization,[5] and numerical renormalization group.[6] Experimentally, however, up to date, only very few examples of clear two-channel Kondo physics have been experimentally realized, e.g., in semiconductor quantum dots,[7] in magnetically doped nanowires, and in metallic glasses.[8,9]

Recently, the Kondo effect of magnetic adatoms in graphene has attracted much attention, theoretically[10,11] as well as experimentally,[12] due to the possible realization of a two-channel Kondo ground state. One interesting aspect of Kondo physics in graphene is due to the Dirac (linear) spectrum that gives rise to a pseudogap local density of states (DOS), $\rho_c(\omega) \propto |\omega|^r$ with $r = 1$, at the impurity site, making graphene one of the few experimental realizations of the pseudogap Kondo model,[13,14] the simplest model to study critical Kondo destruction.[15,16] In the pseudogap Kondo (or more generally Anderson) model, a quantum phase transition is expected between the Kondo screened and the unscreened local moment (LM) ground states for $0 < r < 1$.[14,17] For $r = 1$, corresponding to graphene, Kondo screening does not occur in the particle-hole symmetric case,[11,14,18] resulting in a LM ground state. Nevertheless, Kondo screening can be induced by changing the Fermi energy, e.g., by applying a gate voltage ($\mu \neq 0$).

That two independent screening channels can exist in graphene is related to the existence of two inequivalent Dirac points (K and K') in its band structure. However, the two-channel Kondo physics due to the valleys in graphene seems not likely to occur as there is always backscattering between the valleys, mediated by the impurity. Yet, recent striking scanning tunneling microscopy (STM) measurements done by the Stanford group[12] on Co-doped graphene displayed features in line with two-channel Kondo scaling if the adatom is in the center of the honeycomb lattice. To date, no other similar experiment has provided independent evidence of two-channel Kondo physics in graphene. Whether or not the above-mentioned STM results should be interpreted in terms of two-channel Kondo physics is therefore still under debate and remains controversial (see Sec. IV for details). The situation thus seems reminiscent to that of the possible realization of two-channel Kondo physics in ultrasmall metallic point-contact experiments by Ralph *et al.* where the experimental findings were in line with two-channel Kondo physics but a firm theoretical basis for its occurrence is missing.[19] Compelling evidence in favor of two-channel Kondo physics in the point-contact experiment was recently presented in Ref. 20 by reproducing characteristic conductance spikes in a model realizing two-channel Kondo physics. Motivated by this, we here investigate the nonlinear conductance of a generic two-lead two-channel pseudogap Anderson model with $r = 1$ for putting additional constraints on possible explanations of the experiment reported in Ref. 12.

The two-channel Kondo-LM quantum phase transition in the two-channel pseudogap Kondo and Anderson model with $\mu = 0$ and $0 < r < 1$ in and out of equilibrium has been studied recently,[14,18,21,22] but the experimentally more relevant situation of $r = 1$ and $\mu \neq 0$ has not yet been properly addressed. The possibility of realizing two-channel Kondo physics was pointed out in Ref. 10. There is, however, a lack of systematic investigations beyond the mean-field treatment.

In this paper we focus on the crossover phenomenon from the LM to the two-channel Kondo regime in our model, and work out the universal scaling functions of the conductance. A comprehensive analysis of the nonequilibrium transport, including STM line shapes in the various regimes, is presented.

We address this issue using the noncrossing approximation (NCA),[23–26] which is known to give reliable results for multichannel Kondo systems which are in line with conformal field theory results.[8] It has been shown recently that the NCA

 ©2013 American Physical Society

is able to reproduce the correct qualitative features of the two-channel pseudogap model for $0 \leqslant r \leqslant 1$ in and out of equilibrium in excellent agreement with exact results.[21,22]

Here, we study the steady-state transport properties of the experimentally most relevant pseudogap case, $r = 1$ as a function of doping, temperature, and bias voltage.

II. MODEL HAMILTONIAN

Our starting point is the two-lead two-channel single-impurity pseudogap Anderson model. Each lead is characterized by a power-law density of states (DOS) [$\rho_c(\omega) \sim |\omega| \Theta(D - |\omega|)$, where D is a high-energy cutoff that serves as our unit of energy $D = 1$].

Within a pseudofermion representation, the Hamiltonian reads[24,25]

$$H = \sum_{k,\sigma,\tau,\alpha} (\epsilon_k - \mu_\alpha) c^{\alpha\dagger}_{k\sigma\tau} c^{\alpha}_{k\sigma\tau} + \epsilon_d \sum_{\sigma} f^\dagger_\sigma f_\sigma + \sum_{k,\sigma,\tau,\alpha} \left[U_\alpha \left(f^\dagger_\sigma b_\tau c^{\alpha}_{k,\sigma,\tau} \right) + \text{H.c.} \right], \quad (1)$$

where μ_α is the chemical potential of lead α, and $\alpha = L/R$ labels the two conduction electron leads. The indices σ and τ refer to spin and charge (related to K and K') channels characterizing the conduction electrons. The second and third term on the right-hand side of Eq. (1) represent the spin-1/2 and the hybridization strength U_α between the graphene electrons and the impurity. In the pseudofermion representation the local electron is decomposed as $d^\dagger_{\sigma,\tau} = f^\dagger_\sigma b_\tau$. Equation (1) is a faithful representation of the two-channel single-impurity pseudogap Anderson model, provided the constraint $Q = \sum_\sigma f^\dagger_\sigma f_\sigma + \sum_\tau b^\dagger_\tau b_\tau = 1$ is fulfilled at all times. A finite bias voltage is implemented by shifting the chemical potentials in the leads such that $\mu_L - \mu_R = eV$ is the applied bias voltage across the two-channel Kondo system.

To study the properties of Eq. (1) we employ the NCA. Its ability to correctly capture the properties of the pseudogap two-channel Anderson model was established recently.[21,22] Within the NCA, the retarded self-energy for pseudofermions, $G^r(\omega) = [\omega - \epsilon_d - \Sigma^r(\omega)]^{-1}$, and slave bosons, $D^r(\omega) = [\omega - \Pi^r(\omega)]^{-1}$, are[21,22,24,25]

$$\Sigma^r(\omega) = \frac{2}{\pi} \sum_\alpha \int d\epsilon \Gamma_\alpha(\omega - \epsilon - \mu_\alpha) f(\epsilon - \omega - \mu_\alpha) D^r(\epsilon), \quad (2)$$

$$\Pi^r(\omega) = \frac{2}{\pi} \sum_\alpha \int d\epsilon \Gamma_\alpha(\epsilon - \omega - \mu_\alpha) f(\epsilon - \omega - \mu_\alpha) G^r(\epsilon). \quad (3)$$

The NCA expressions for the lesser self-energy of the pseudofermion, $G^<(\omega) = \Sigma^<(\omega)|G^r(\omega)|^2$, and slave boson, $D^<(\omega) = \Pi^<(\omega)|D^r(\omega)|^2$, are

$$\Sigma^<(\omega) = \frac{2}{\pi} \sum_\alpha \int d\epsilon \Gamma_\alpha(\omega - \epsilon - \mu_\alpha) f(\omega - \epsilon - \mu_\alpha) D^<(\epsilon), \quad (4)$$

$$\Pi^<(\omega) = \frac{2}{\pi} \sum_\alpha \int d\epsilon \Gamma_\alpha(\epsilon - \omega - \mu_\alpha) f(\omega - \epsilon + \mu_\alpha) G^<(\epsilon). \quad (5)$$

Here, $\Gamma_\alpha(\omega) \equiv \Gamma_\alpha \rho_{c,\alpha}(\omega)$ with $\Gamma_\alpha = \pi |U_\alpha|^2$ with $\rho_{c,\alpha}(\omega) \propto |\omega - \mu_\alpha|$ and $f(\omega) = [1 + e^{\beta\omega}]^{-1}$ is the Fermi function.

The physical spectral function, $\rho(\omega, V)$, is the convolution of pseudofermion and slave-boson Green function

$$\rho(\omega, V) = \frac{i}{2\pi^2 Z} \int d\epsilon [\text{Im} D^r(\epsilon) G^<(\omega + \epsilon) - D^<(\epsilon) \text{Im} G^r(\omega + \epsilon)]. \quad (6)$$

The normalization factor $Z = \frac{i}{\pi} \int d\omega [D^<(\omega) - G^<(\omega)]$ enforces the constraint $\langle Q \rangle = 1$. The current is given by[27]

$$I(V,T) = \frac{2e}{\hbar} \int d\omega \frac{2\Gamma_L(\omega)\Gamma_R(\omega)}{\Gamma_L(\omega) + \Gamma_R(\omega)} \rho(\omega, V, T) \times [f(\omega + eV/2) - f(\omega - eV/2)]. \quad (7)$$

The nonlinear conductance $G(V) = dI(V)/dV$ is computed by numerical derivative of the current $I(V)$, whereas the linear-response conductance is directly obtained from

$$G(0,T) = \frac{2e^2}{\hbar} \int d\omega \frac{2\Gamma_L(\omega)\Gamma_R(\omega)}{\Gamma_L(\omega) + \Gamma_R(\omega)} \left(- \frac{\partial f(\omega)}{\partial \omega} \right) \times \rho(\omega, V = 0). \quad (8)$$

Equations (4) and (5) together with the Dyson equation for $G(\omega)$ and $D(\omega)$ form a self-consistent set of integral equations. These equations are iterated until a solution is found with which Eqs. (6)–(8) can be evaluated.

III. RESULTS

We now turn to a discussion of the self-consistent solution of Eqs. (2)–(5); the results are summarized in the phase diagram Fig. 1. For simplicity, we focus on the particularly simple case with parity (left-right) symmetry, $U_L = U_R$, $\Gamma_L = \Gamma_R \equiv \frac{\Gamma}{2}$.

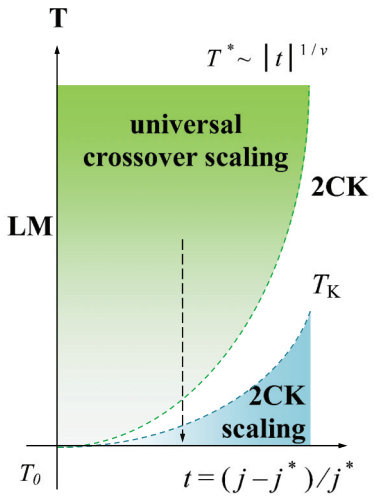

FIG. 1. (Color online) Schematic phase diagram for the crossover between two-channel Kondo and local moment phase in our generic model Eq. (1). The parameter j refers to either Γ or μ (in units of $D = 1$), and j^* refers to the crossover scale for a fixed temperature $T_0 \sim 5 \times 10^{-7} D$. T_K and T^* represent crossover energy scales associated with the universal scaling for the two-channel Kondo (blue shaded) and the high-temperature 2CK-LM crossover scaling (green shaded) regime, respectively.

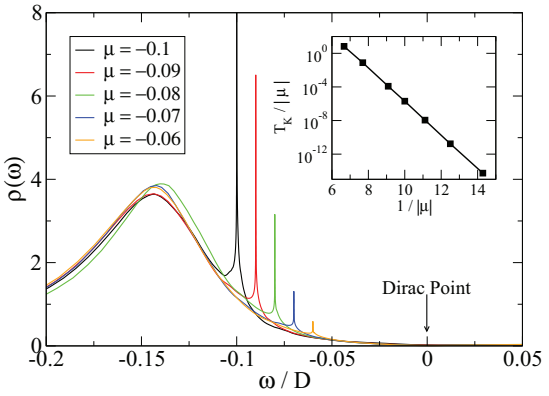

FIG. 2. (Color online) The impurity spectral function $\rho(\omega)$ vs chemical potential μ (in units of the bandwidth D). The Kondo peak is pinned near μ. The Dirac point is assigned $\omega = 0$. Inset: Kondo temperature T_K (defined in text) as a function of μ. The NCA parameters are $T = 5 \times 10^{-7}D$, $\Gamma = 0.2D$, $\epsilon_d = -0.2D$.

For larger values of $j = \Gamma, |\mu|$ (or $j - j^* > 0.1D$) with $\Gamma^* \sim 0.05D$ and $\mu^* \sim -0.05D$ being crossover scales at a fixed temperature $T_0 \sim 10^{-7}D$, our results show clear two-channel Kondo behaviors at low temperatures $T < T_K$ where T_K is the Kondo temperature defined as the temperature where $G(0,T)$ deviates from a $\sim \sqrt{T}$ behavior,[25] in agreement with its conventional definition: $G(0,T_K) = G(0,0)/2$.

However, for smaller values of j with $j - j^* < 0.1D$, we find universal power-law scaling of $G(T,0)$ distinct from both two-channel Kondo (i.e., $\sim \sqrt{T}$) and one-channel Kondo (i.e., $\sim T^2$) (Ref. 28) behavior at temperatures $T \gg T^*$ where T^* is the crossover energy scale, describing the two-channel Kondo-LM crossover. Note that the NCA gives reliable results for $I(V,T)$ even in the single-channel Kondo case as long as $T \gtrsim 0.1T_K$.

The crossover scale is finite for any nonvanishing gate voltage ($\mu \neq 0$). We checked that the crossover scales $\Gamma^*, |\mu^*|$ vanish as $T \to 0$ in a power-law fashion, consistent with the general expectation that Kondo screening in graphene can be induced by arbitrarily small doping ($\mu \neq 0$).

The local density of states $\rho(\omega, V)$, given by Eq. (6), is shown in Fig. 2. The Kondo peaks occur at the chemical potential μ, and the Kondo temperature T_K follows the pseudogap Kondo behavior with $r = 1$: $T_K \sim |\mu| \times e^{(-a/|\mu|)}$ (inset in Fig. 2) where a has the unit of energy and is a function of the bandwidth D and the Kondo coupling J.[13] The $|\omega|$ decay in the vicinity of $\omega = 0$ is a reflection of the Dirac point of the conduction electrons with DOS $\rho_c(\omega) \sim |\omega|$. Comparable results have also been discussed in Refs. 11 and 29–32.

Figures 3(a) and 3(b) shows the linear-response conductance $G(0,T)$ obtained via numerical derivative of Eqs. (7) and (8). As long as $\mu \neq 0$, we find clear two-channel Kondo behavior at the low-temperature regime [Fig. 3(a)], with $G(0,T)$ displaying a $T^{1/2}$ behavior for each coupling Γ.[25] The Kondo temperature T_K behaves as $T_K \sim De^{-\pi|\epsilon_d|/\Gamma}$ [Fig. 3(a) inset]. For higher temperatures [Fig. 3(b)], we find a universal power-law behavior in T/T^* for $T > T^*$ near $\Gamma^* \approx 0.05D$: $G(0,T) \propto (T/T^*)^\alpha$ with $\alpha \approx 0.029$, indicating the universal crossover from two-channel Kondo to LM regime. The

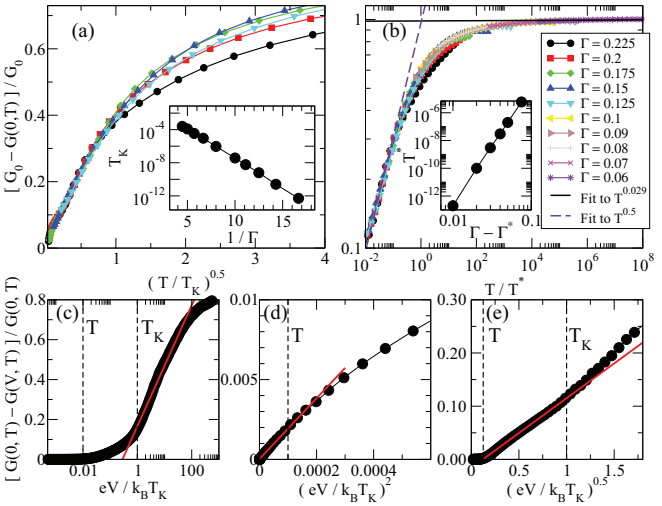

FIG. 3. (Color online) (a) $[G_0 - G(0,T)]/G_0$ calculated from Eq. (8) displays $T^{1/2}$ behavior for $T < T_K$. $G_0 \equiv G(0,T_0)_{\Gamma=0.225D}$ is the linear conductance at the lowest numerically accessible temperature $T_0 \approx 5 \times 10^{-7}D$ at $\Gamma = 0.225D$. Inset: Exponential behavior for $T_K \sim De^{-\pi|\epsilon_d|/\Gamma}$. (b) An additional power-law behavior at high temperature for small $\Gamma \approx \Gamma^* \approx 0.05D$, where the crossover scale T^* shows a power-law behavior $T^* \sim |\Gamma - \Gamma^*|^{1/\nu}$ with $\nu \sim 0.1$ (inset). Here, $\epsilon_d = -0.2D$, $\mu = -0.1D$. (c)–(e) Nonlinear conductance at a large $\Gamma = 0.2D$, and fixed parameters $T_0 = 5 \times 10^{-7}D$, $\mu = -0.1D$, $\epsilon_d = -0.2D$. The $G(V,T)$ curve shows two-channel Kondo behavior: (c) $\ln V$ dependence around $V \sim T_K$ with $T_K \approx 5 \times 10^{-5}D$ and $T = T_0$. (d) V^2 behavior for $V < T$. (e) $T^{1/2}$ two-channel Kondo behavior for $T < V < T_K$. Here, the red lines are fits to the corresponding power-law or logarithmic behaviors in different bias regime.

crossover energy scale T^* shows a power-law dependence, $T^* \sim |\Gamma - \Gamma^*|^{1/\nu}$ [Fig. 3(b) inset], where $\nu \sim 0.1$.

$G(V,T)$ at larger Γ shows clear two-channel Kondo behavior [see Figs. 3(c)–3(e) for $\Gamma = 0.2D$]. Figure 3(c) indicates the $\ln V$ behavior predicted for Kondo scattering processes. The V^2 behavior at $V < T$ and $V^{1/2}$ behavior at $T < V < T_K$ in Figs. 3(d) and 3(e), respectively, are the characteristics of two-channel Kondo physics.

To illustrate the crossover between the two-channel Kondo and LM regimes, $G(V,T)$ is shown in Figs. 4 and 5. Figure 4 demonstrates V/T scaling[33] of $G(V,T)$ for $\Gamma = 0.07D$ and $\mu = -0.08D$. The resulting curves collapse onto a universal function. For $V/T > 10^2$, $G(V,T)$ shows a power-law behavior similar to the one shown in Fig. 3(b); for $1 < V/T < 10$, the behavior follows the two-channel Kondo $V^{1/2}$ behavior as shown in the inset of Fig. 4; for $V \ll T$, it shows V^2 Fermi-liquid behavior. Figure 5(a) is the two-channel Kondo scaling plot for large Γ, where all curves follow the scaling function[25] $G(0,T) - G(V,T) = B_\Sigma T^{1/2} H(A\frac{eV}{T_K})$. Here, $H(x) \propto x^{1/2}$ is a universal function and B_Σ and A are nonuniversal constants.[25] For $V > V^*$, $G(V,T)$ shows the same universal two-channel Kondo-LM power-law crossover behavior for small coupling $\Gamma \approx \Gamma^*$ as shown in the linear conductance, $G(0,T)$: $G(0,T) - G(V,T) \propto (V/V^*)^\alpha$ with $\alpha \approx 0.029$ [see Fig. 5(b)]. The crossover energy scale V^*

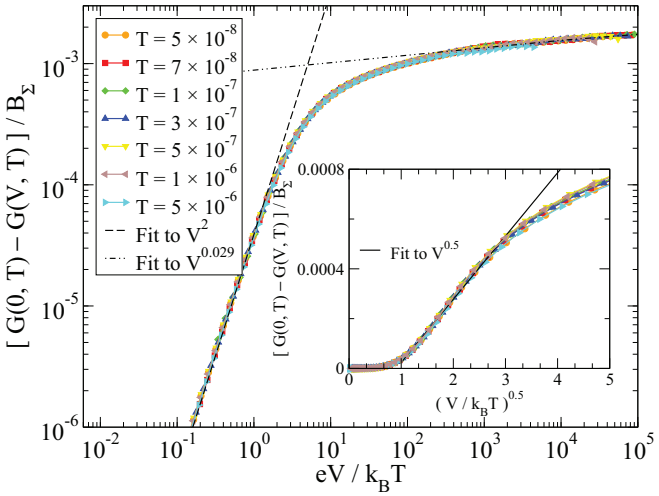

FIG. 4. (Color online) Temperature scaling of the nonlinear conductance $G(V,T)$ in the universal crossover region with $\Gamma = 0.07D$ and $\mu = -0.08D$ ($\epsilon_d = -0.2D$). All curves collapse onto a universal scaling function. It displays $V^{1/2}$ behavior at $T < V < 10T$ (inset). For large V (in units of D), $V/T > 10^2$, $G(V,T)$ shows a power-law behavior similar to Fig. 3(d).

also displays a power-law behavior $V^* \sim |\Gamma - \Gamma^*|^{1/\nu}$, where $\nu \sim 0.1$, in line with the equilibrium behavior.

IV. APPLICATIONS FOR CO-DOPED GRAPHENE VIA STM

As mentioned above, due to the two inequivalent Dirac points (K and K') in graphene, it therefore was argued that the effective low-energy model for magnetic impurities in graphene depends on the location of the adatom:[34] if the impurity is located at the center of the cell, the intervalley

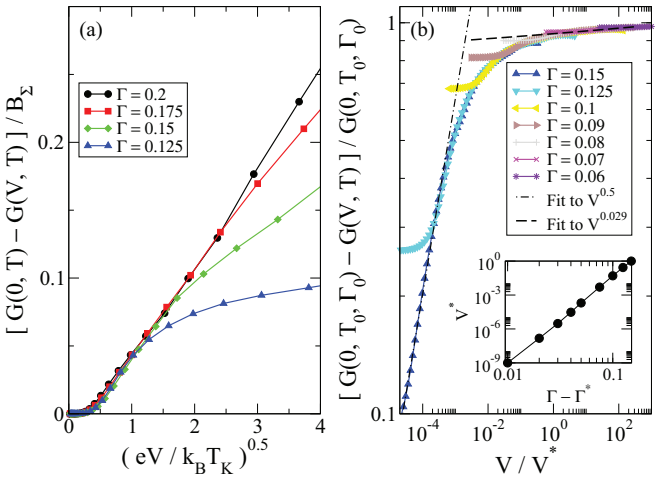

FIG. 5. (Color online) (a) Scaling of $G(V,T)$ for large Γ (parameters are the same as in Fig. 2). For $V < T_K$, $G(V,T)$ collapses onto a single curve $\sim T^{1/2}$. (b) Power-law behavior of $G(V,T)$ for $V > V^*$. Here, $G(0,T_0,\Gamma_0)$ refers to the linear conductance at a fixed temperature $T_0 = 5 \times 10^{-7} D$ and a fixed coupling $\Gamma_0 = 0.2D$. Inset: Power-law behavior of the crossover energy scale $V^* \sim |\Gamma - \Gamma^*|^{\alpha}$ (see text). Here, $\epsilon_d = -0.2D$, $\mu = -0.1D$.

scattering does not couple the two screening channels and an effective two-channel Kondo ensues.[10] This has been explicitly demonstrated within a tight-binding description where the hybridization between electronic states in graphene and impurity states preserves the A-B sublattice symmetry.[35] The situation is different if the adatom is located on a graphene site and the sublattice symmetry is absent in the impurity-graphene hybridization. The effective low-energy model is in this case the more conventional one-channel pseudogap Kondo model.[34,35] The difference between the various adatom positions can be probed by scanning tunneling microscopy (STM).[36] This has been achieved recently with Co atoms as magnetic adatoms where signatures of two-channel Kondo physics are seen when the adatom is located at the zone center of the honeycomb cell such that the intervalley scatterings between K and K' Dirac electrons are strongly suppressed.[12]

However, the claim that the two valleys in graphene should give rise to a two-channel Kondo effect when the adatom sits in the center of the honeycomb cell is based on the tight-binding analysis in the continuum,[34,35] which might not be valid at the lattice scale. In fact, by computing the spin exchange interaction at the tight-binding level the authors in Refs. 37 and 38 show that the Kondo Hamiltonian corresponding to magnetically doped graphene can be rotated into a new basis where only one channel is coupled. Therefore, the two-channel Kondo physics due to the valleys in graphene seems unlikely at the lattice scale as there is always backscattering between the valleys, which is mediated by the impurity.

Based on the above two different analyses leading to two different conclusions, the issue of whether or not one should expect two-channel Kondo physics in graphene at a finite temperature or energy scale needs further studies and clarification. Here we try to put a stringent constraint on the possible two-channel Kondo physics in graphene based on the NCA approach to the nonlinear out-of-equilibrium transport in the two-lead two-channel pseudogap Anderson model with $r = 1$. Our results may serve as references for future experimental works on this topic. Below we apply our general formalism on the model for the STM setup for Co-doped graphene in Ref. 12. To make contact with Ref. 12, it is necessary to generalize our setup to the case where one of the leads is made up of a simple (i.e., one-channel) metal with constant DOS $\rho_{\rm tip}$ near its Fermi energy. The ground state in this case will be that of a Fermi liquid. If, however, the tip is coupled only very weakly ($\Gamma_{\rm tip}/D \ll 1$) to the magnetic adatom on graphene, the corresponding energy scale will be vanishingly small. In this case it is permissible to replace the normal-metal lead by a two-channel lead (with constant DOS at the Fermi energy), as the RG equations for the one-channel and two-channel Kondo problem coincide in lowest order. The two-channel Kondo physics is expected to have relevance for the transport at low temperatures and/or finite bias voltages.

A. Nonequilibrium NCA

The extension of the noncrossing approximation (NCA) onto the Keldysh contour has been discussed in several papers.[24,25] It is customary to neglect the bias voltage dependence of the conduction electron density of states (DOS) $\rho(\epsilon)$. This is justified provided ρ is well approximated by a

constant in a region around the Fermi energy that is large compared to the applied bias voltage. When the DOS vanishes in a power-law fashion at or near the Fermi energy, this is no longer possible and the equations have to be generalized appropriately. The full set of equations to be solved for the two-channel pseudogap problem becomes

$$\Sigma_B^<(\omega) = (-2i)\int_{-\infty}^{\infty} d\epsilon\, G_f^<(\epsilon+\omega)[|V_L|^2 f(-\epsilon+\mu_L)\rho_L(\epsilon-\mu_L-\mu)+|V_R|^2 f(-\epsilon+\mu_R)\rho_R(\epsilon-\mu_R-\mu)]$$
$$\Sigma_B^>(\omega) = 2i\int_{-\infty}^{\infty} d\epsilon\, G_f^>(\epsilon+\omega)[|V_L|^2 f(\epsilon-\mu_L)\rho_L(\epsilon-\mu_L-\mu)+|V_R|^2 f(\epsilon-\mu_R)\rho_R(\epsilon-\mu_R-\mu)]$$

for the pseudoboson and

$$\Sigma_f^<(\omega) = 2i\int_{-\infty}^{\infty} d\epsilon\, G_B^<(\epsilon+\omega)[|V_L|^2 f(-\epsilon+\mu_L)\rho_L(-\epsilon+\mu_L+\mu)+|V_R|^2 f(-\epsilon+\mu_R)\rho_R(-\epsilon+\mu_R+\mu)]$$
$$\Sigma_f^>(\omega) = 2i\int_{-\infty}^{\infty} d\epsilon\, G_B^>(\epsilon+\omega)[|V_L|^2 f(\epsilon-\mu_L)\rho_L(-\epsilon+\mu_L+\mu)+|V_R|^2 f(\epsilon-\mu_R)\rho_R(-\epsilon+\mu_R+\mu)]$$

for the pseudofermion. The DOS (ρ_L and ρ_R) of the two leads does not have to be identical. The bias voltage applied across the system is $eV^{\rm bias} = \mu_L - \mu_R$, where μ_L and μ_R are the chemical potentials of the left and right leads.

B. Fano line shapes

An experiment reminiscent of the situation considered by us has been performed recently, where magnetic adatoms on graphene were investigated via scanning tunneling microscopy (STM); see Ref. 12. Our analysis can be extended to include the current-voltage characteristics measured by an STM (see Fig. 6). In this case, one of the two fermionic leads represents the STM tip and it is necessary to explicitly allow for the different tunneling paths between the STM tip, the adatom, and the substrate which will act as the second lead. An important difference between the STM setup and our analysis so far is that the STM tip is a *good* metal, e.g., a single-channel lead with constant DOS at its Fermi energy. We here will model it by a two-channel lead with constant DOS at its Fermi energy. This is justified provided the coupling between the STM tip and the system is small as the RG scaling equations for the two- and one-channel case are identical up to fourth order in the tunneling matrix element.

The theory of STM on magnetic adatoms on a metal surfaces has been worked out by Schiller and Hershfield[39]

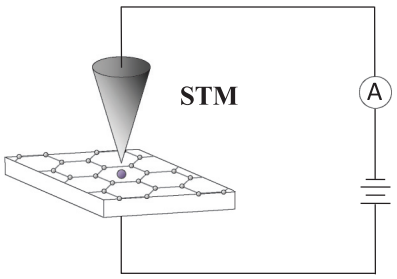

FIG. 6. The STM measurement of the magnetic adatom in graphene. The $S = 1/2$ magnetic adatom is located at the center of the honeycomb lattice of graphene.

and by O. Újsághy *et al.*[40] The current is obtained from

$$I(V) \sim \int_{-\infty}^{\infty} d\epsilon [f(\epsilon - eV^{\rm bias}) - f(\epsilon)]\rho_{\rm tip}\rho_{\rm eff}(\epsilon), \quad (9)$$

where $\rho_{\rm tip}$ is the density of states of the STM tip and $\rho_{\rm eff}$ is an effective density of states probed by the STM and depends on two tunneling rates t_f and t_c that parametrize the hybridization strength of the STM tip with the magnetic adatom (t_f) and the graphene leads (t_c). The effective density of states $\rho_{\rm eff}$ can be recast into

$$\rho_{\rm eff} = \frac{1}{\pi}{\rm Im}\{t_c^2 G_c(\vec{R},\vec{R},\epsilon) + [t_d + t_c V G_c(\vec{R},\vec{R}_{ad},\epsilon)] \times G_{ad}(\epsilon)[t_d + t_c V^* G_c(\vec{R}_{ad},\vec{R},\epsilon)]\}, \quad (10)$$

where V is the hybridization strength between the graphene electrons and the magnetic adatom $G_c(\epsilon)$ is the advanced local graphene electron Green function at the locus of the STM tip $\vec{R}$ and $G_c(\vec{R},\vec{R}_{ad},\epsilon)$ is the advanced graphene electron Green function connecting the locus of the tip with the position of the adatom at $\vec{R}_{ad}$, and t_c (t_d) is the tunneling matrix element between the STM tip and the substrate (magnetic adatom). $G_{ad}(\epsilon)$ is the advanced Green function of the magnetic adatom that can be obtained from the pseudoparticle Green functions of section **A**.

In the linear regime, the Fano line shape is given by the differential conductance $dI/dV|_{V\to 0}$, which turns out to be proportional to the effective density of states $\rho_{\rm eff}(\epsilon)$: $dI/dV|_{V\to 0} \propto \rho_{\rm eff}(\epsilon = V)$.

$dI/dV|_{V\to 0}$ can be cast into the Fano line shape where the Fano parameter q is given by[40–43]

$$q = -\frac{{\rm Re}G_c^0(\epsilon - i\eta)}{{\rm Im}G_c^0(\epsilon - i\eta)}, \quad (11)$$

and can be treated as approximately constant in the energy range of interest.[41]

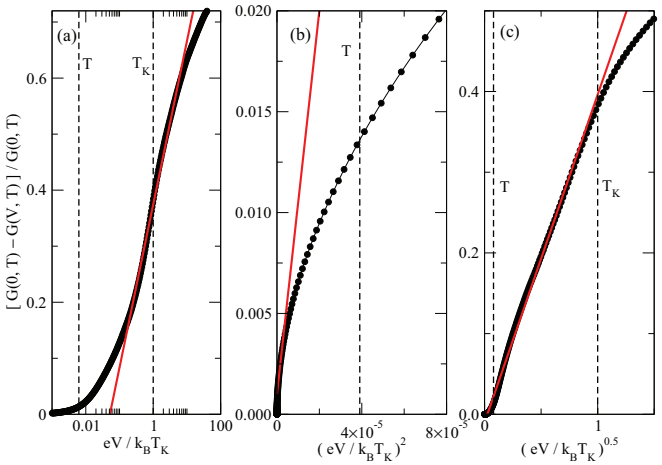

FIG. 7. (Color online) Nonlinear conductance for a large $\Gamma = 0.1D$ between impurity and graphene substrate and a much smaller hopping Γ_{ts} between tip and the impurity, $\Gamma_{st} \ll \Gamma$, corresponding to the STM measurement reported in Ref. 12. The $G(V,T)$ curves agree well with the STM results of Ref. 12. (a) $\ln V$ dependence around $V \sim T_K$. (b) V^2 behavior for $V < T$. (c) $T^{1/2}$ two-channel Kondo behavior for $T < V < T_K$. Here, $T = 5 \times 10^{-7} D$. The other parameters are $\mu = -0.1D$, $\epsilon_d = -0.2D$.

C. Results: Universal two-channel Kondo-LM crossover for $\mu < 0$

The behavior of $G(V,T)$ in this case is shown in Fig. 7, compatible with the results discussed above, see, e.g., Figs. 3(c)–3(e). These results are in line with the experimental findings reported in Ref. 12. Typical Fano line shapes in the linear regime are shown in Fig. 8. The two-channel Kondo behavior seen in the STM measurement[12] for Co adatom at the center of the honeycomb lattice is signaled by the Kondo peaks at $\omega = \mu$ in Fano line shapes, which are compatible with a large fitting parameter q (for example $q = 10$) and a correspondingly small t_c/t_d and concomitantly small intervalley scattering.

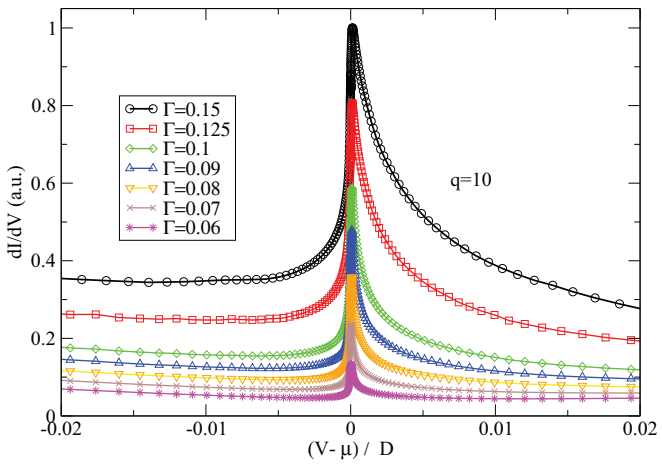

FIG. 8. (Color online) Fano line shapes with Fano parameter $q = 10$ for various values of Γ (in units of the half bandwidth D). Here, we have set $\epsilon_d = -0.2D$, $\mu = -0.1D$.

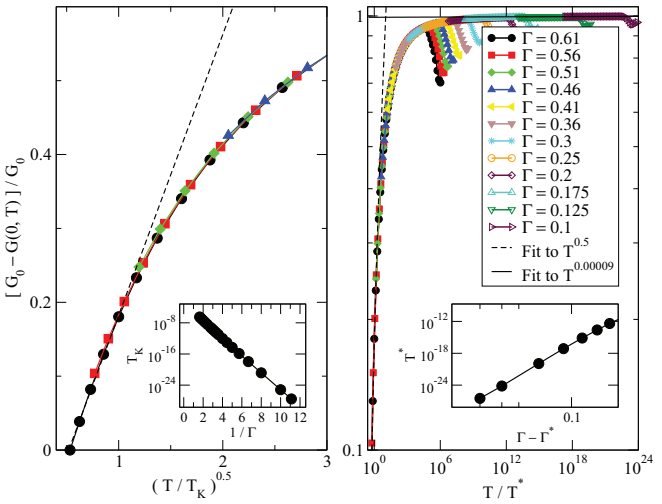

FIG. 9. (Color online) Universal scaling in linear conductance $G(T)$ as a function of temperature T for at fixed positive chemical potential $\mu = 0.1D$ and for various values of hybridization Γ. (a) $T^{1/2}$ two-channel Kondo behavior for $T < T_K$ for large values of Γ. Inset: T_K/Γ vs $1/\Gamma$. (b) Universal scaling of $G(T)$ for smaller values of Γ. Inset: The crossover energy scale T^* as a power-law function of $\Gamma - \Gamma^*$. Here, $\epsilon_d = -0.2D$, G_0 is the linear conductance for $\Gamma = 0.62D$ at $T = 5 \times 10^{-7} D$, and $\Gamma^* \approx 0.06D$.

D. Results: Universal two-channel Kondo-LM crossover for $\mu > 0$

In the previous sections, we focus on the universal two-channel Kondo-LM crossover for negative chemical potential, $\mu < 0$. A similar scaling behavior can also be found in conductance for positive μ. As shown in Fig. 9, for a fixed positive $\mu = 0.1D$, the linear conductance $G(T)$ vs hybridization Γ follows a single universal scaling form of T/T^*. The single scaling form of $G(T)$ we observe here for $\mu > 0$ is somewhat surprising as for $\mu < 0$ the conductance shows two distinct scaling regimes: $T < T_K$ and $T > T^*$. We believe that this difference maybe due to the particle-hole asymmetry in our model as the Kondo peak, located at $\omega = \mu$, is affected more by the charge peak at $\epsilon_d < 0$ for $\mu < 0$ than that for $\mu > 0$.

Similar to the case for $\mu < 0$, the linear conductance for $\mu > 0$ shows a typical two-channel Kondo $\sqrt{T}$ behavior for $T < T_K$, and a universal power-law behavior at high temperatures for $\Gamma \to \Gamma^*$: $G(T) \propto (T/T^*)^\alpha$ with $\alpha \approx 0.000\,09 \approx 0$. The Kondo temperature T_K and the crossover scale T^* for $\mu > 0$ behave in a similar way to their $\mu < 0$ counterparts: $T_K \propto \Gamma \times e^{-1/\Gamma}$, $T^* \propto (\Gamma - \Gamma^*)^{1/\nu}$ with $\Gamma^* \approx 0.06D$ and $\nu \sim 0.05$. We believe that our results for both positive and negative values of μ could be used as theoretical guidance in future experiments to clarify the issue on two-channel Kondo physics in graphene.

V. CONCLUSIONS

Universal out-of-equilibrium scaling is currently pursed in a wide range of condensed-matter systems. As demonstrated, magnetic adatoms on graphene offer the possibility to study steady-state properties in a universal crossover regime of a two-channel Kondo/Anderson model. Whether or not

two-channel Kondo physics is relevant for the magnetic adatoms on graphene needs further investigations. Here, we have addressed the universal crossover regime that separates the local moment regime from the two-channel Kondo regime in a generic two-lead two-channel pseudogap Anderson model with $r = 1$. In particular, we calculated the differential conductance both in the linear and nonlinear regime. For sufficiently large hybridization, we found clear two-channel Kondo signatures. As the hybridization is reduced, the crossover region separating two-channel Kondo and local moment ground states is entered and the crossover is monitored by the narrowing of the Kondo resonances. In the crossover regime, the conductance shows universal power-law behavior. Our results seem to be consistent with a recent scanning tunneling spectroscopy experiment. We also provide a comprehensive theoretical analysis of the transport properties of two-channel Kondo impurities in graphene.

ACKNOWLEDGMENTS

We thank T. Chowdhury, K. Ingersent, J. Kroha, K. Sengupta, P. Ribeiro, F. Zamani, M. Vojta, and in particular H. Manoharan for useful discussions. C.H.C. acknowledges NSC Grants No. 98-2112-M-009-010-MY3 and No. 101-2628-M-009-001-MY3, the NCTS, and the MOE-ATU program of Taiwan R.O.C.

[1] A. C. Hewson, *The Kondo Problem to Heavy Fermions* (Cambridge University Press, Cambridge, UK, 1997).
[2] P. Nozieres and A. Blandin, J. Phys. (Paris) **41**, 193 (1980).
[3] N. Andrei and C. Destri, Phys. Rev. Lett. **52**, 364 (1984); P. B. Wiegmann and A. M. Tsvelik, J. Stat. Phys. **38**, 125 (1985).
[4] I. Affleck and A. W. W. Ludwig, Nucl. Phys. B **352**, 849 (1991); **360**, 641 (1991); A. W. W. Ludwig and I. Affleck, Phys. Rev. Lett. **67**, 3160 (1991).
[5] V. J. Emery and S. Kivelson, Phys. Rev. B **46**, 10812 (1992); M. Fabrizio and A. O. Gogolin, *ibid.* **51**, 17827 (1995).
[6] A. K. Mitchell, E. Sela, and D. E. Logan, Phys. Rev. Lett. **108**, 086405 (2012).
[7] R. M. Potok, I. G. Rau, H. Shtrikman, Y. Oreg, and Goldhaber-Gordon, Nature (London) **446**, 167 (2007).
[8] D. L. Cox and A. Zawadowski, Adv. Phys. **47**, 599 (1998).
[9] T. Cichorek, A. Sanchez, P. Gegenwart, F. Weickert, A. Wojakowski, Z. Henkie, G. Auffermann, S. Paschen, R. Kniep, and F. Steglich, Phys. Rev. Lett. **94**, 236603 (2005).
[10] K. Sengupta and G. Baskaran, Phys. Rev. B **77**, 045417 (2008).
[11] Matthias Vojta, Lars Fritz, and Ralf Bulla, Europhys. Lett. **90**, 27006 (2010).
[12] L. S. Mattos, Ph.D. thesis, Stanford University, 2009.
[13] D. Withoff and E. Fradkin, Phys. Rev. Lett. **64**, 1835 (1990).
[14] C. Gonzalez-Buxton and K. Ingersent, Phys. Rev. B **57**, 14254 (1998).
[15] K. Ingersent and Q. Si, Phys. Rev. Lett. **89**, 076403 (2002).
[16] M. T. Glossop, S. Kirchner, J. H. Pixley, and Q. Si, Phys. Rev. Lett. **107**, 076404 (2011).
[17] L. Fritz and M. Vojta, Phys. Rev. B **70**, 214427 (2004).
[18] I. Schneider, L. Fritz, F. B. Anders, A. Benlagra, and M. Vojta, Phys. Rev. B **84**, 125139 (2011).
[19] D. C. Ralph and R. A. Buhrman, Phys. Rev. Lett. **69**, 2118 (1992); D. C. Ralph, A. W. W. Ludwig, Jan von Delft, and R. A. Buhrman, *ibid.* **72**, 1064 (1994).
[20] M. Arnold, T. Langenbruch, and J. Kroha, Phys. Rev. Lett. **99**, 186601 (2007).
[21] F. Zamani, T. Chowdhury, P. Ribeiro, K. Ingersent, and S. Kirchner, Phys. Status Solidi B **250**, 547 (2013).
[22] F. Zamani, T. Chowdhury, P. Ribeiro, K. Ingersent, and S. Kirchner, (unpublished).
[23] D. L. Cox and A. E. Ruckenstein, Phys. Rev. Lett. **71**, 1613 (1993).
[24] N. S. Wingreen and Y. Meir, Phys. Rev. B **49**, 11040 (1994).
[25] M. H. Hettler, J. Kroha, and S. Hershfield, Phys. Rev. Lett. **73**, 1967 (1994).
[26] M. Vojta, Phys. Rev. Lett. **87**, 097202 (2001).
[27] Y. Meir and Ned S. Wingreen, Phys. Rev. Lett. **68**, 2512 (1992).
[28] M. Grobis, I. G. Rau, R. M. Potok, H. Shtrikman, and D. Goldhaber-Gordon, Phys. Rev. Lett. **100**, 246601 (2008).
[29] P. S. Cornaglia, G. Usaj, and C. A. Balseiro, Phys. Rev. Lett. **102**, 046801 (2009).
[30] Huai-Bin Zhuang, Qing-feng Sun, and X. C. Xie, Europhys. Lett. **86**, 58004 (2009).
[31] Z. G. Zhu and J. Berakdar, Phys. Rev. B **84**, 165105 (2011).
[32] L. Li, Y.-Y. Ni, Y. Zhong, T.-F. Fang, and H.-G. Luo, New J. Phys. **15**, 053018 (2013).
[33] S. Kirchner and Q. Si, Phys. Rev. Lett. **103**, 206401 (2009).
[34] L. Dell'Anna, J. Stat. Mech. (2010) P01007.
[35] Z.-G. Zhu, K.-H. Ding, and J. Berakdar, Europhys. Lett. **90**, 67001 (2010).
[36] T. O. Wehling, H. P. Dahal, A. I. Lichtenstein, M. I. Katsnelson, H. C. Manoharan, and A. V. Balatsky, Phys. Rev. B **81**, 085413 (2010).
[37] B. Uchoa, T. G. Rappoport, and A. H. CastroNeto, Phys. Rev. Lett. **106**, 016801 (2011).
[38] E. Kogan, Phys. Rev. B **84**, 115119 (2011).
[39] A. Schiller and S. Hershfield, Phys. Rev. B **61**, 9036 (2000).
[40] O. Újsághy, J. Kroha, L. Szunyogh, and A. Zawadowski, Phys. Rev. Lett. **85**, 2557 (2000).
[41] U. Fano, Phys. Rev. **124**, 1866 (1961).
[42] C.-H. Chung and T.-H. Lee, Phys. Rev. B **82**, 085325 (2010).
[43] V. Madhavan, W. Chen, T. Jamneala, M. F. Crommie, and N. S. Wingreen, Phys. Rev. B **64**, 165412 (2001).